Tomographic image of melt storage beneath Askja Volcano, Iceland using local microseismicity

Michael A. Mitchell,[1,2] Robert S. White,[1] Steve Roecker,[3] and Tim Greenfield[1]

Received 17 June 2013; revised 22 August 2013; accepted 22 August 2013; published 3 October 2013.

[1] We use *P* wave and *S* wave arrivals from microseismic earthquakes to construct 3-D tomographic V_p and V_s images of the magma storage region beneath Askja's central volcano in the Northern Volcanic Zone of Iceland. A distinctive ellipsoidal low-velocity anomaly, with both V_p and V_s velocities 8–12% below the background, is imaged at 6–11 km depth beneath the caldera. The presence of a shallow magma chamber is corroborated by geodetic and gravity studies. The small V_p/V_s anomaly suggests a lack of pervasive melt. We interpret this anomaly as a region of multiple sills, some frozen but hot, others containing partial melt. A second, smaller low-velocity anomaly beneath the main magma storage region may represent a magma migration pathway. This interpretation is supported by the close proximity to the anomaly of clusters of deep, magmatically induced earthquakes. However, the location and shape of this deep anomaly are poorly constrained by the current data set. **Citation:** Mitchell, M. A., R. S. White, S. Roecker, and T. Greenfield (2013), Tomographic image of melt storage beneath Askja Volcano, Iceland using local microseismicity, *Geophys. Res. Lett.*, *40*, 5040–5046, doi:10.1002/grl.50899.

1. Introduction

[2] Iceland is formed where the mid-Atlantic ridge has been elevated above sea level as a result of thickened crust and dynamic support from the underlying mantle plume. Rifting and volcanism occur within three main neovolcanic zones (inset, Figure 1). The volcanic zones are subdivided into local volcanic systems, most of which contain a central volcano crosscut by a fissure swarm. This study focuses on the Askja central volcano (sometimes called the Dyngjufjöll volcanic center) [*Sigvaldason*, 2002], which lies in the southern part of the Northern Volcanic Zone (NVZ) and contains a series of three overlapping calderas. Combined, these calderas cover an area of approximately 45 km^2. Regional seismic refraction studies, receiver function analysis, and gravity modeling estimate the crustal thickness beneath the Askja volcanic system to be 30–35 km [*Wolfe et al.*, 1997; *Darbyshire et al.*, 2000].

[3] The youngest caldera, Öskjuvatn, is partly filled by a lake and was formed during Askja's most recent volcano-tectonic rifting episode in 1875–1876. This episode consisted of a large explosive, rhyolitic, subPlinian-phreatoplinian-Plinian eruption in March 1875, most likely resulting from an intrusion of basaltic magma into an older, more silicic reservoir [*Sigurdsson and Sparks*, 1981]. It was accompanied by a series of effusive, basaltic eruptions approximately 60 km to the north in the Sveinagjá graben from February to November 1875. During the early 20th century, a series of small basaltic eruptions and one fissure eruption occurred around the caldera. Öskjuvatn reached its present size (approximate dimensions: 4.3 km (East-West) by 3.2 km (North-South) with a maximum depth of 217 m) in the 1930s following an estimated 2.88 km^3 of subsidence over more than 40 years [*Hartley and Thordarson*, 2012].

[4] More recent activity includes a small fissure eruption from the Askja caldera in December 1961 which produced a 9 km long lava flow that breached the northern caldera rim. Although there has not been any volcanic activity at Askja since the 1961 eruption, surface expressions of geothermal activity are still present around Öskjuvatn caldera. Generally, only a few percent, or at most a few tens of percent, of the melt in a magma chamber is removed during an explosive eruption [*Bower and Woods*, 1997], so it is likely that there remains a considerable quantity of melt beneath the caldera today.

[5] Recent geodetic [*Sturkell et al.*, 2006; *Pagli et al.*, 2006; *Dickinson et al.*, 2009; *Pedersen et al.*, 2009] and gravity [*de Zeeuw-van Dalfsen et al.*, 2005] based studies in Askja suggest the presence of a shallow (c. 3 km deep) magma chamber beneath the caldera. In this study, we analyze records of microearthquakes recorded by a local seismometer network to attempt to image the extent of this magma chamber using seismic arrival time tomography. By developing a more complete image of Askja's subcaldera magma chamber and its associated magmatic plumbing, researchers can gain important insights into the volcano's formation, evolution, and current state of activity.

2. Data Acquisition and Processing

[6] Since July 2006 we have maintained a network of broadband (0.04–50 Hz) Guralp 6TD three-component seismometers around the Askja caldera (Figure 1). In this study we analyze arrival times of *P* and *S* waves from earthquakes recorded by this network from 2007 to 2011, supplemented by observations from the Icelandic Meteorological Office. Of the 1185 earthquakes used in the inversion, 313 are newly picked, while the remaining arrival times were picked by

Additional supporting information may be found in the online version of this article.

[1]Department of Earth Sciences, Bullard Laboratories, University of Cambridge, Cambridge, UK.

[2]Now at Department of Earth, Ocean, and Atmospheric Sciences, Geophysical Inversion Facility (GIF), University of British Columbia, Vancouver, British Columbia, Canada.

[3]Department of Earth and Environmental Sciences, Rensselaer Polytechnic Institute, Troy, New York, USA.

Corresponding author: M. A. Mitchell, Department of Earth, Ocean and Atmospheric Sciences, Geophysical Inversion Facility (GIF), University of British Columbia, Earth Sciences Building, 2207 Main Mall, Vancouver, BC V6T 1Z4, Canada. (mmitchel@eos.ubc.ca)

0094-8276/13/10.1002/grl.50899

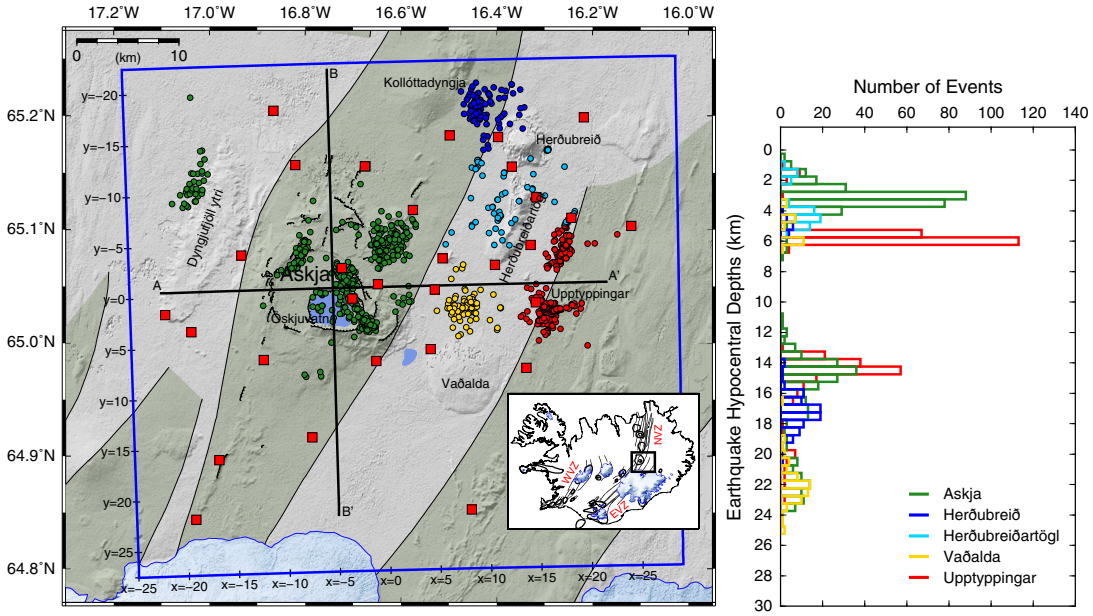

Figure 1. Locations of seismometers (red squares), and earthquakes (colored dots) around Askja used for tomographic inversion. Earthquakes are color coded by region with Askja, green; Herðubreið, dark blue; Herðubreiðartögl, light blue; Vaðalda, yellow; and Upptyppingar, red. The olive green shaded regions show the extent of mapped fissure swarms, and the superimposed grid shows local coordinates used for tomographic inversion. The depth distribution of hypocenters is shown in histogram to the right of the map. Inset shows regional map of Iceland with small rectangle marking the study region and fine lines showing the main rift zones: WVZ-Western Volcanic Zone; EVZ-Eastern Volcanic Zone; NVZ-Northern Volcanic Zone.

Key et al. [2011], *Martens et al.* [2010], and *White et al.* [2011]. Because the resolution and reliability of the final tomographic model is dependent on the number and orientation of raypaths penetrating each model cell [e.g., *Lees*, 2007], events were selected to maximize the spatial distribution. Nevertheless, unavoidable gaps in the microseismicity remain (Figure 1).

[7] Following the selection process, the arrival times were put through a rigorous manual phase pick refinement process to improve their accuracy. We estimate the average uncertainties of P and S arrival times to be 0.025 s and 0.05 s, respectively.

3. Velocity Model Inversion

3.1. Regional 1-D Velocity Model

[8] In order to have a reasonable starting model for 3-D tomography, we inverted the data set of microseismic arrival times using VELEST, a damped least squares based inversion program that can invert for hypocentral locations, station corrections, and a 1-D velocity model simultaneously [*Kissling et al.*, 1994]. Due to the interdependent nature of hypocentral locations, station corrections, and the velocity model, we attempted numerous inversions, with varying input and control parameters, to produce a stable and geologically reasonable velocity model. The resulting velocity models are similar to those developed in previous studies, although V_p and V_s velocities at depths between 16 and 31 km are consistently 2–5% higher than those determined by *Martens et al.* [2010] and *Key et al.* [2011] (Table S2 in the supporting information), which were derived from two regional seismic refraction surveys in the vicinity: ICEMELT [*Darbyshire et al.*, 1998] and RRISP [*Gebrande et al.*, 1980; *Menke et al.*, 1996]. The model developed by *Martens et al.* [2010] and *Key et al.* [2011] will be referred to as the Askja regional velocity model.

[9] To check the self-consistency of the VELEST derived 1-D velocity model, a series of 1-D reference models were created using both the VELEST results and the results from previous studies. After completing an iteration of the 3-D tomographic inversion using each of these separate starting models, the resulting data misfit statistics were compared and the model which minimized the data misfit was selected as the optimal 1-D velocity model (see Table S1). Figure 2 shows that this optimal 1-D reference model is similar to Askja's regional velocity model [*Key et al.*, 2011; *Martens et al.*, 2010; *Darbyshire et al.*, 1998; *Gebrande et al.*, 1980; *Menke et al.*, 1996] (see Table S1) with the exception of the V_p and V_s velocities at depths between 16 and 31 km that are approximately 3–4% faster. This optimal 1-D velocity model was used as the starting model for the tomographic inversion presented in this paper, and the percent changes in velocity are referenced to this model.

3.2. The 3-D Tomographic Inversion

[10] The 3-D tomographic inversion code used in this study is essentially the same as that previously used to image the velocity structure of the San Andreas Fault near Parkfield, California [*Roecker et al.*, 2006] and the western Tien Shan [*Zhiwei et al.*, 2009]. Travel times and raypaths are computed using a finite difference eikonal equation solver based on the methodology of *Vidale* [1988] as described by *Hole and Zelt* [1995]. This approach provides better accuracy in highly heterogeneous environments and decreases the likelihood of stagnating in a local travel time minima [*Roecker et al.*, 2006]. P and S velocities are specified at a

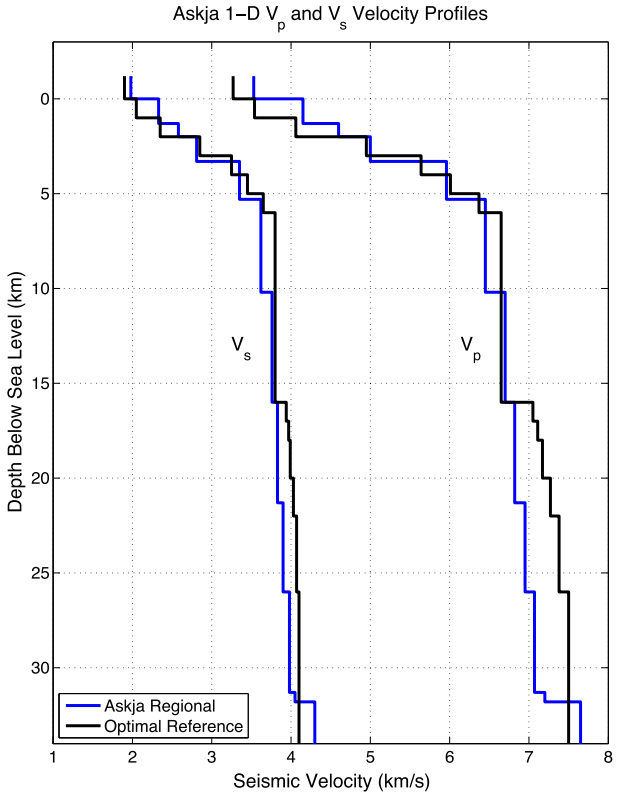

Figure 2. A comparison of our optimal 1-D reference velocity model (black lines) with the Askja regional velocity model (blue lines) developed by *Martens et al.* [2010] and *Key et al.* [2011] from two regional seismic refraction surveys in the vicinity: ICEMELT [*Darbyshire et al.*, 1998] and RRISP [*Gebrande et al.*, 1980; *Menke et al.*, 1996]. All depths are in kilometers below sea level with Askja's caldera rim reaching its highest point at –1.516 km. As this plot shows, there is a high degree of correlation between the two models, although the optimal reference model has slightly higher V_p and V_s velocities between 16 and 32 km depth. Since it is difficult to decipher the exact values for depths and velocities plotted here, the same models are presented in tabular form within the supporting information (see Tables S1 and S2).

mesh of nodes and estimated at any point in the model by trilinear interpolation. We chose a grid spacing of 1 km, based on the anticipated level of resolution of the data set. Model perturbations are determined by a simultaneous inversion of velocities and hypocenters using the LSQR algorithm of *Paige and Saunders* [1982]. Hypocenters are relocated in the current model and the procedure iterates until changes in the variance of the arrival time residuals are insignificant.

[11] To mitigate the introduction of artifacts, a three-cell wide moving-average window is applied after each iteration to reduce the amplitude of small-scale features. We chose a damping parameter which allows the data misfit and model perturbations to decrease steadily at each iteration. Generally, we found that nine iterations were required before the variance reduction became insignificant as shown in Figure 3. The final variance is 0.0046 s^2, which is a 41% reduction from the initial variance but still well above the variance expected from the uncertainties in the arrival times (0.0016 s^2).

[12] In the process of obtaining a final tomographic model, more than 50 trials were run using different 1-D reference velocity models, damping parameters, and data subsets to ensure that possible sources of bias were identified and that the resulting images were consistent. Since the inversion code has the ability to solve for either V_p and V_p/V_s or V_p and V_s, trials were performed using both settings. These trials produced very similar results, thus increasing our confidence in the large-scale model structures. When solved for independently, variations in V_s closely track those of V_p, and only minor variations result from inversions for V_p/V_s. Because of this similarity, only the V_p model is presented in the main article. The V_s and V_p/V_s models are shown in Figures S1 and S2. The presented models were produced by solving for V_p and V_p/V_s. Since there are fewer S wave arrival time picks and they typically have larger uncertainties than the P wave arrival time picks, we expect the V_p model to have better resolution than the V_s or V_p/V_s models.

4. Results

[13] The most prominent feature in the tomographic model (Figures 4 and 5, and S3) is a 8–12% negative velocity anomaly beneath the Askja caldera. This anomaly extends approximately 6–11 km in depth and is roughly 6 km wide in both the E-W and N-S directions (Figure 4). A smaller low-velocity anomaly extends beneath the main low velocity body between 13–19 km depth.

[14] We interpret the uniformly lower V_p and V_s in the main anomaly as evidence of a shallow magma chamber. However, since only a slight elevation in V_p/V_s is observed beneath the caldera, and S waves are detected from many raypaths that cut through the low-velocity region, it is likely that much of the velocity anomaly is caused by high, but subsolidus temperature rock with melt distributed in many small sills rather than in a single large magma chamber.

[15] Based on its shape and location beneath the shallow magma storage region, and its close proximity to clusters of

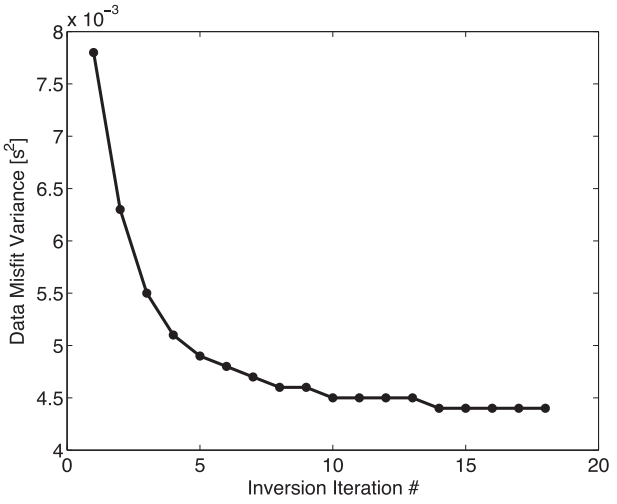

Figure 3. A plot of the data misfit variance as a function of inversion iteration. After approximately 8–10 iterations, the variance no longer decreases significantly with additional iterations. Further iterations increase the structural complexity of the model by requiring the addition of small-scale anomalies which may be artifacts.

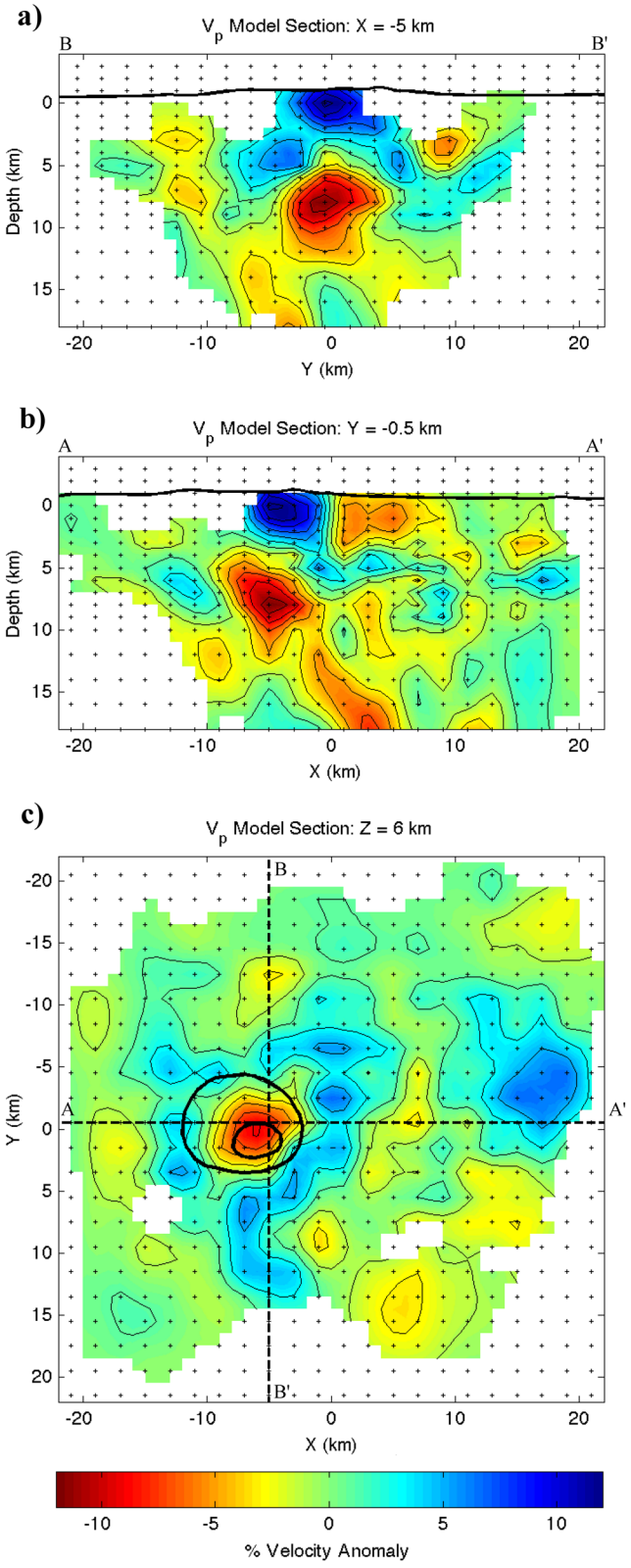

Figure 4. Panels showing x, y, and z sections of the tomographic model (V_p velocities) that slice through the imaged magma chamber anomaly. (a) A north-south section along x = –5 km; (b) An east-west section along y = –0.5 km; and (c) A depth slice from z = 6 km. Figure 4c also shows an outline of the Askja and Öskjuvatn calderas (solid black lines) and the location of the x and y sections (broken black lines). Only cells with a ray hit count above 10 are colored.

deep earthquakes that have been associated with movement of magma within the lower crust [*Soosalu et al.*, 2010; *Key et al.*, 2011], we suggest that the smaller and deeper anomaly represents a magma migration pathway within the crust, possibly as an active/partially crystallized dyke system by which magma injected into the lower crust is fed into the shallow magma storage region. At the same time, the size and geometry of this anomaly are not well constrained by the current data set, so this interpretation is somewhat speculative.

[16] In addition to the low-velocity anomalies, a shallow, 5–10% high velocity anomaly is also imaged directly beneath the caldera. It is possible that high-density lava flows within the caldera have produced a near surface, high velocity core [*Brown et al.*, 1991]. Alternatively, this structure could be a high velocity dome such as the one imaged beneath Krafla by *Brandsdóttir et al.* [1997]. Since high-velocity domes are not characteristic of volcanic centers along the mid-Atlantic ridge, they may be a feature that develops as part of the interplay between the calderas and transecting rift zones of Iceland.

[17] We estimate the resolution of the final tomographic model by determining how well the procedure recovers different synthetic models. Two such models were created: a standard checker board model (see Figure S4) and a magma chamber model (see Figure 6). Synthetic phase arrival time data sets were generated using the same hypocentral

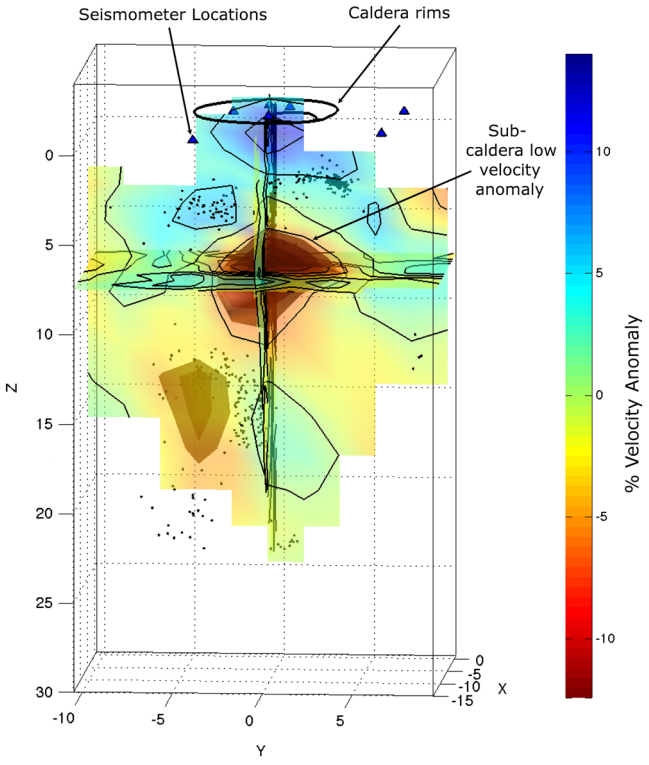

Figure 5. View of the final tomographic model looking east on intersecting N-S and E-W sections. The –5.75% V_p velocity isosurface encloses the imaged magma storage region beneath the caldera. Earthquake hypocenters are plotted as black dots in this 3-D view. Note the halo of earthquakes that lie above the shallow, subcaldera low-velocity anomaly. The animation (provided in the supporting information, Figure S3) shows a 360° rotation of this rendering to better visualize spatial relationships.

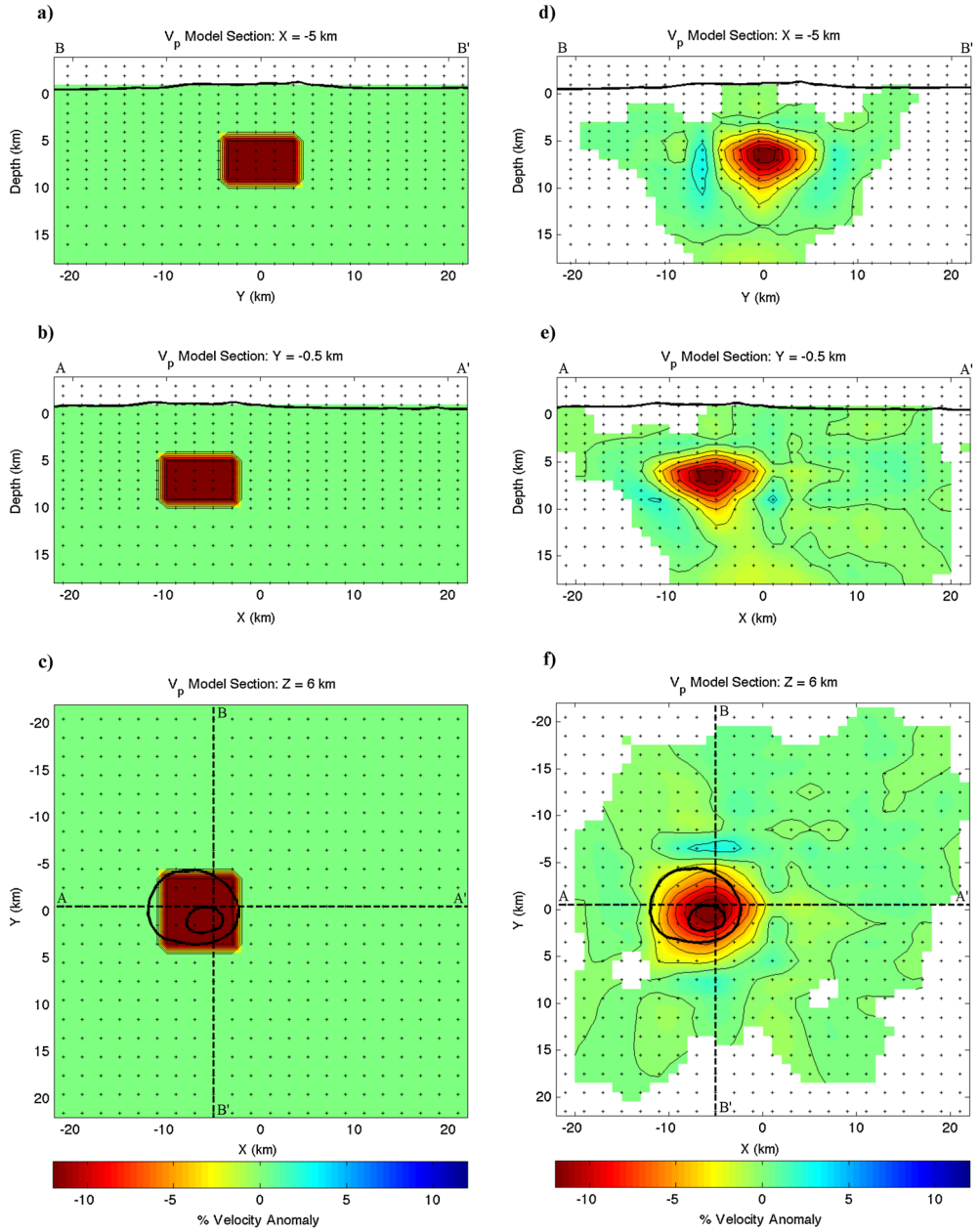

Figure 6. Results of the magma chamber recovery test with three cross sections passing through the inferred magma chamber beneath the Askja caldera. (a) x, (b) y, and (c) z sections through the true model; (d, e, f) the corresponding recovered model sections. As in the results of the checker board recovery test shown in Figure S4, these test results indicate that the model resolution in the region where the shallow, subcaldera low-velocity anomaly was detected is good enough to reliably characterize the magma chamber's location, size, and velocity contrast.

earthquake distribution and station locations as used in the inversion. These data sets were analyzed in the same manner as the real data, using the same 1-D starting model, damping parameters, grid cell size, and data/station distribution, to determine how well the resulting tomographic model could recover velocity anomalies in different parts of the model.

[18] The synthetic checkerboard model contains a series of uniformly distributed 4 km by 4 km prisms with an alternating positive and negative velocity contrast of 5% with respect to the starting 1-D reference model. Since the checkerboard model has an even distribution of anomalies throughout, it is a useful tool for evaluating spatial variations in model resolution. The checkerboard test results (see Figure S4) show that the data set and procedure are capable of resolving spatial variations on the order of a few kilometers within the core survey region. In the southern and western portions of the model, resolution decreases due to a lack of adequate ray coverage. Since only slight differences are observed between the recovered V_p and V_s checkerboard models, the resolution of the V_s model is not significantly lower than that of the V_p model.

[19] The magma chamber recovery test (Figure 6) assesses the robustness of the magma chamber image identified in the final tomographic model. The synthetic model is a single rectangular prism that is similar in size, spatial location, and velocity contrast (–10% with respect to the 1-D

starting model) to the shallow, subcaldera, low-velocity anomaly imaged in the shallow magma storage region. As shown in Figure 6, the maximum amplitude of the magma chamber anomaly is well recovered, as is the spatial location of its center. Based on this result, however, it would seem that the inversion slightly underestimates the size and thickness of the anomaly, putting the center point roughly 0.5 km shallower than it actually is. Directly beneath the magma chamber anomaly, there is an apparent pull-down effect that creates a small tongue of low velocity (velocity contrast of approximately –3%) material which extends to a depth of about 12 km, while some slightly positive anomalies (0–2%) ring the magma chamber in map view. Despite these minor artifacts, the main features of the anomaly associated with the magma storage region are well recovered. The lack of a high velocity anomaly above the magma chamber anomaly in this test suggests that the shallow high velocity anomaly imaged beneath the caldera is a real structure and not an artifact of the inversion.

5. Conclusions

[20] The final tomographic model shows the presence of a 8–12% low-velocity anomaly beneath the Askja caldera which extends from 6 to 11 km depth (Figures 4 and 5). Due to the absence of a large V_p/V_s anomaly, we interpret this anomaly to be a magma storage region containing high, but subsolidus temperature rock with melt distributed in many small sills rather than in a single large magma chamber.

[21] The imaged magma storage region is deeper than the 3 km suggested by GPS and InSAR based subsidence modeling using a point Mogi source [*Sturkell et al.*, 2006; *Pagli et al.*, 2006], but its center is in a similar position, under the northern edge of Öskjuvatn. The presence of shallow seismicity within the caldera extending down to a depth of 4–5 km supports this deeper location of the magma chamber since microseismicity, which is likely induced by geothermal activity, would not be expected to occur in the region of magma storage itself but in the cooler more brittle rock above it. The halo of shallow seismicity above the magma storage region can be seen in Figure 5 and in the 3-D volume rotation (Figure S3).

[22] The absence of a deeper low-velocity anomaly around 16 km depth, where a second magma chamber has been proposed from Mogi source inversions [*Sturkell et al.*, 2006; *Pagli et al.*, 2006], supports models which suggest that geodynamic processes associated with rifting can be used to account for the regional deformation not accommodated by a shallow magma chamber [*Dickinson et al.*, 2009; *Pedersen et al.*, 2009]. Moreover, the inversion result provides some evidence to support the existence of a melt transport system extending from the clusters of deep earthquakes [*Soosalu et al.*, 2010; *Key et al.*, 2011], induced by the injection of magma into the lower crust, up toward the northern edge of the magma storage region. However, while this inference is intriguing, we note that model resolution decreases significantly below 15 km and additional data should be collected and analyzed to investigate this feature further.

[23] **Acknowledgments.** Seismometers were borrowed from the Natural Environment Research Council SEIS-UK on loans 857 and 914. Data from station MKO was kindly made available by the Icelandic Meteorological Office. We thank all those who have assisted in fieldwork and data analysis since 2006, and especially Janet Key, Hilary Martens, Jon Tarasewicz, and Heidi Soosalu. Additional thanks go to Janet Key and Hilary Martens for allowing us to incorporate a large number of their refined phase arrival picks into this inversion. We would also like to thank Michele Paulatto and an anonymous reviewer for their insightful and constructive comments. Figure 1 was produced using Generic Mapping Tools (GMT). Dept. of Earth Sciences, Cambridge contribution ESC.2858.

[24] The Editor thanks two anonymous reviewers for their assistance in evaluating this paper.

References

Brandsdóttir, B., W. H. Menke, P. Einarsson, R. S. White, and R. K. Staples (1997), Faroe-Iceland Ridge Experiment 2. Crustal structure of the Krafla central volcano, *J. Geophys. Res.*, *102*(B4), 7867–7886.

Bower, S. M., and A. W. Woods (1997), Control of magma volatile content and chamber depth on the mass erupted during explosive volcanic eruptions, *J. Geophys. Res.*, *102*, 10,273–10,290.

Brown, G. C., S. P. Everett, H. Rymer, D. W. McGarvie, and I. Foster (1991), New light on caldera evolution-Askja, Iceland, *Geology*, *19*, 352–355.

Darbyshire, F. A., I. T. Bjarnason, R. S. White, and O. G. Flóvenz (1998), Crustal structure above the Iceland mantle plume imaged by the ICEMELT refraction profile, *Geophys. J. Int.*, *135*(3), 1131–1149.

Darbyshire, F. A., R. S. White, and K. F. Priestley (2000), Structure of the crust and uppermost mantle of Iceland from a combined seismic and gravity study, *Earth Sci. Front.*, *181*(3), 409–428.

de Zeeuw-van Dalfsen, E., H. Rymer, F. Sigmundsson, and E. Sturkell (2005), Net gravity decrease at Askja volcano, Iceland: Constraints on processes responsible for continuous caldera deflation, 1988–2003, *J. Volcanol. Geotherm. Res.*, *139*, 227–239.

Dickinson, H., T. Masterlark, K. L. Feigl, R. Pedersen, and F. Sigmundsson (2009), Finite element models for the deformation of the Askja volcanic complex and rift segment, Iceland, *Eos Trans. AGU*, *90*(52).

Gebrande, H., H. Miller, and P. Einarsson (1980), Seismic structure of Iceland along the RRISP-Profile, *Int. J. Geophys.*, *47*, 239–249.

Hartley, M., and T. Thordarson (2012), Formation of Öskjuvatn caldera at Askja, North Iceland: Mechanism of caldera collapse and implications for the lateral flow hypothesis, *J. Volcanol. Geotherm. Res.*, *227–228*, 85–101.

Hole, J. A., and B. C. Zelt (1995), 3-D finite-difference reflection traveltimes, *Geophys. J. Int.*, *121*(2), 427–434.

Key, J., R. S. White, H. Soosalu, and S. S. Jakobsdóttir (2011), Multiple melt injection along a spreading segment at Askja, Iceland, *Geophys. Res. Lett.*, *38*(5), 1–5, doi:10.1029/2010GL046264.

Kissling, E., W. L. Ellsworth, D. Eberhart-Phillips, and U. Kradolfer (1994), Initial reference models in local earthquake tomography, *J. Geophys. Res.*, *99*, 19,635–19,646.

Lees, J. M. (2007), Seismic tomography of magmatic systems, *J. Volcanol. Geotherm. Res.*, *167*(1–4), 37–56.

Martens, H. R., R. S. White, J. Key, J. Drew, H. Soosalu, and S. S. Jakobsdóttir (2010), Dense seismic network provides new insight into the 2007 Upptyppingar dyke intrusion, *Jökull*, *60*, 47–66.

Menke, W., B. Brandsdóttir, P. Einarsson, and I. T. Bjarnason (1996), Reinterpretation of the RRISP-77 Iceland shear-wave profiles, *Geophys. J. Int.*, *126*(1), 166–172.

Pagli, C., F. Sigmundsson, T. Arnadóttir, P. Einarsson, and E. Sturkell (2006), Deflation of the Askja volcanic system: Constraints on the deformation source from combined inversion of satellite radar interferograms and GPS measurements, *J. Volcanol. Geotherm. Res.*, *152*(1–2), 97–108.

Paige, C. C., and M. A. Saunders (1982), LSQR: An algorithm for sparse linear equations and sparse least squares, *ACM Trans. Math. Software*, *8*(1), 43–71.

Pedersen, R., F. Sigmundsson, and T. Masterlark (2009), Rheologic controls on inter-rifting deformation of the Northern Volcanic Zone, Iceland, *Earth Environ. Sci. Trans.*, *281*(1–2), 14–26.

Roecker, S., C. Thurber, K. Roberts, and L. Powell (2006), Refining the image of the San Andreas Fault near Parkfield, California using a finite difference travel time computation technique, *Tectonophysics*, *426*(1–2), 189–205.

Sigurdsson, H., and R. S. J. Sparks (1981), Petrology of rhyolitic and mixed magma ejecta from the 1875 eruption of Askja, Iceland, *J. Petrol.*, *22*, 41–84.

Sigvaldason, G. (2002), Volcanic and tectonic processes coinciding with glaciation and crustal rebound: An early Holocene rhyolitic eruption in the Dyngjufjöll volcanic centre and the formation of the Askja caldera, north Iceland, *Bull. Volcanol.*, *64*, 192–205.

Soosalu, H., J. Key, R. S. White, C. Knox, P. Einarsson, and S. S. Jakobsdóttir (2010), Lower-crustal earthquakes caused by magma movement beneath Askja volcano on the north Iceland rift, *Bull. Volcanol.*, *72*(1), 55–62.

Sturkell, E., F. Sigmundsson, and R. Slunga (2006), 1983–2003 decaying rate of deflation at Askja caldera: Pressure decrease in an extensive

magma plumbing system at a spreading plate boundary, *Bull. Volcanol.*, *68*(7–8), 727–735.

Vidale, J. (1988), Finite-difference calculation of travel times, *Bull. Seismol. Soc. Am.*, *78*(6), 2062–2076.

White, R. S., J. Drew, H. R. Martens, J. Key, H. Soosalu, and S. S. Jakobsdóttir (2011), Dynamics of dyke intrusion in the mid-crust of Iceland, *Earth Planet. Sci. Lett.*, *304*, 300–312.

Wolfe, C., I. T. Bjarnason, J. C. VanDecar, and S. C. Solomon (1997), Seismic structure of the Iceland mantle plume, *Nature*, *385*, 245–247.

Zhiwei, L., S. Roecker, L. Zhihai, W. Bin, W. Haitao, G. Schelochkov, and V. Bragin (2009), Tomographic image of the crust and upper mantle beneath the western Tien Shan from the MANAS broadband deployment: Possible evidence for lithospheric delamination, *Tectonophysics*, *477*(1–2), 49–57.